The Astronomical Journal, 167:279 (7pp), 2024 June https://doi.org/10.3847/1538-3881/ad4704

Surviving Tidal Tails Around the Milky Way Bulge Globular Cluster NGC 6355

Andrés E. Piatti[1,2]
[1] Instituto Interdisciplinario de Ciencias Básicas (ICB), CONICET-UNCUYO, Padre J. Contreras 1300, M5502JMA, Mendoza, Argentina; andres.piatti@fcen.uncu.edu.ar
[2] Consejo Nacional de Investigaciones Científicas y Técnicas (CONICET), Godoy Cruz 2290, C1425FQB, Buenos Aires, Argentina
Received 2024 March 7; revised 2024 April 19; accepted 2024 May 1; published 2024 May 23

Abstract

We present results of the analysis of a set of images obtained in the field of the Milky Way bulge globular cluster NGC 6355 using the Dark Energy Camera, which is attached to the 4 m Blanco telescope of the Cerro-Tololo Interamerican Observatory. We dealt with a heavy differential absorption across the observed field, a crowded field star population, and the superposition of field stars on to the cluster color–magnitude diagram main features to produce an intrinsic cluster stars density map. The resulting stellar density map reveals the presence of an extended envelope, a tidal tail, and scattered debris; the tidal tails pointing toward the Milky Way center. Such extra-tidal overdensities, detected above the mean star field density, resulted to be between four and six times larger that the local star field density fluctuation. They have also been recently generated by two independent studies which performed numerical simulations of synthetic tidal tails of Milky Way globular clusters. These results contrast with previous theoretical speculations about the possibility to detect tidal tails of globular clusters with chaotic orbits because they would be washed out after they were generated.

Unified Astronomy Thesaurus concepts: Globular star clusters (656); Astronomical techniques (1684); Galactic bulge (2041)

1. Introduction

Recently, Callingham et al. (2022) chemo-dynamically established a group of 42 globular clusters that belong to the Milky Way bulge. None of them is included in the stringent compilation of Milky Way globular clusters with studies of their extra-tidal structures (Zhang et al. 2022). These extra-tidal features are fundamental for our understanding of their association with destroyed dwarf progenitors (Carballo-Bello et al. 2014; Mackey et al. 2019), whether they formed in dark matter minihaloes (Starkman et al. 2020; Baumgardt & Vasiliev 2021; Wan et al. 2021), and their dynamical history as a consequence of the interaction with the Milky Way (Hozumi & Burkert 2015; de Boer et al. 2019; Piatti & Carballo-Bello 2020), among others. These topics result in compelling motivations to detect and characterize tidal tails in bulge globular clusters.

Tidal tail stars are those no longer bound to the globular cluster where they formed, and because of that they are located beyond the cluster Jacobi radius (r_J). In order to abandon the cluster, they have increased their velocities, so that their escape velocities differentiate from the velocities of cluster members. For this reason, looking for tidal tail stars from proper motions with values similar to the mean cluster proper motion could be misleading. Projection effects of the tidal tails, the intrinsic kinematic agitation of the tidal tail (Wan et al. 2023), and the Milky Way gravitational interaction can additionally make the proper motions of tidal tail stars different from the mean cluster proper motion. Conversely, it is possible to find field stars projected along the cluster line of sight that share proper motions similar to cluster stars (Piatti et al. 2023). For instance, Sollima (2020) claim the detection of high significance tails around NGC 7099 using Gaia DR2 proper motions (Gaia Collaboration et al. 2018; Lindegren et al. 2018), while Piatti et al. (2020) did not reproduce these using the deep Dark Energy Camera (DECam; Flaugher et al. 2015) photometry.

Two main different processes are thought to be responsible for stars to escape a globular cluster; namely, two-body relaxation, and tidal effects caused by the Milky Way's gravitational field (Piatti et al. 2019, and reference therein). Hence, searches for tidal tail stars have long been focused on faint main-sequence stars (low-mass stars) because they are more numerous (Carballo-Bello et al. 2012). However, when dealing with bulge globular clusters, and particularly with those affected by heavy differential interstellar absorption, reaching the cluster low main sequence could be a defying challenge for wide-field ground imaging (Kader et al. 2023). Additionally, searching tidal tails from filtering stars along the cluster color–magnitude diagram is constrained by the contamination of field stars located along the cluster features. This is because it is not possible to select a field star comparison field to decontaminate the cluster color–magnitude diagram with the certainty a priori that it does not contain cluster tidal tail stars. Precisely, the composite stellar population toward the Milky Way bulge is highly dominated by field stars superimposed on to the cluster main sequences (Gran et al. 2022).

In this study we report the detection of tidal tails around the Milky Way bulge globular cluster NGC 6355, which was recently analyzed in detail by Souza et al. (2023) from high-resolution spectroscopy and Hubble Space telescope imaging. NGC 6355 is a 13.2 ± 1.1 Gyr old bulge globular cluster with a mean metallicity $[Fe/H] = -1.39 \pm 0.08$ dex, placed at a distance of 8.54 ± 0.19 kpc from the Sun. In Section 2 we present the wide-field observational data obtained to investigate the existence of tidal tails in the outskirts of the cluster. In Section 3 we build a cluster stellar density map, while in Section 4 we discuss the resulting extra-tidal structures. In Section 5 we summarize the main conclusions of this work.

2. Observational Data

We obtained a collection of images with DECam (Flaugher et al. 2015), which assembles 62 identical chips with a scale of 0.263 arcsec pixel^{-1}, thus providing a 3 deg^2 field of view. DECam is attached to the prime focus of the 4 m Blanco telescope at the Cerro Tololo Inter-American Observatory (CTIO). The images with a quality better than 0.6 arcsec were taken as part of the observing program 2023A-627924 (PI: A. Piatti) and consist of 4×400 s g and 1×250 s $+$ 2×400 s i exposures, respectively. The image processing was fully conducted by the DECam community pipeline team, which applied the highest performance instrumental calibrations, and managed any peculiar image behavior. Among the tasks carried out on the images are trimming of bad edge pixels, generating reference bias and dome flat files taken for the observing night to remove the instrumental signature from the science data, resampling the images to a standard orientation and pixel scale at a standard tangent point, and performing photometric calibrations.

The finally processed images were used to build a master table containing for each measured source the equatorial coordinates, g and i magnitudes with their respective errors, sharpness, and χ values. We assigned R.A. and decl. coordinates using the WCSTOOL package.[3] In order to measure g and i magnitudes, we split the DECam images into nine equal squared areas of ∼0.67 deg per side, thus performing robust quadratically spatially varying point-spread function (PSF) fitting for each subfield. In doing this, we used the DAOPHOT/ALLSTAR suite of programs (Stetson et al. 1990) and two groups of PSF stars selected interactively, with ∼2200 stars deg^2 and 900 stars deg^2, respectively. The later contains the brightest, least contaminated PSF stars used to generate a preliminary PSF, which in turn was used to eliminate neighboring stars from the former PSF group, and thus obtain a final clean fitted PSF. We applied the resulting PSF to identified sources in each subfield using the ALLSTAR program, iterating the process three times from images generated by subtracting known sources to measure magnitudes of fainter stars. We matched g- and i-image tables using the IRAF.IMMATCH@WCSMAP task, and then stand-alone DAOMATCH/DAOMASTER routines.[4] With the aim of removing bad pixels, unresolved double stars, cosmic rays, and background galaxies from the photometric catalog, we kept 888941 sources with |sharpness| <0.5.

We corrected the resulting photometry from interstellar absorption using the $E(B-V)$ values according to the positions of the stars in the sky and using the A_λ/A_V coefficients given by Wang & Chen (2019). The $E(B-V)$ values were obtained by interpolation in the interstellar extinction map built by Schlafly & Finkbeiner (2011), provided by the NASA/IPAC Infrared Science Archive[5] for the entire analyzed area. Figure 1 shows the relative large variation of relatively high $E(B-V)$ values across the observe cluster region. We used the reddening corrected magnitudes and colors to produce Figure 2, which illustrates the distribution of the measured stars in the color–magnitude diagram. Figure 2 highlights the cluster's color–magnitude diagram features. We used all the measured stars located within a circle of radius equal to three times the cluster's half-mass–radius ($r_h = 0.022$ deg; Piatti et al. 2019) in order to minimize the field contamination. Figure 2 also shows that the photometric uncertainties of magnitude and color for the faintest observed cluster's stars are smaller than ∼0.05 mag. NGC 6355 appears projected onto a crowded star field (gray dots in Figure 2).

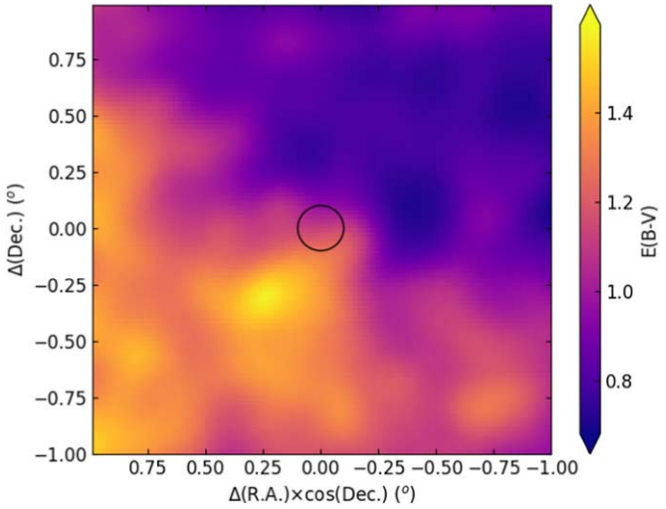

Figure 1. Interstellar extinction ($E(B-V)$) map across the observed NGC 6355 field. The black circle represents the cluster radius Piatti et al. (2019).

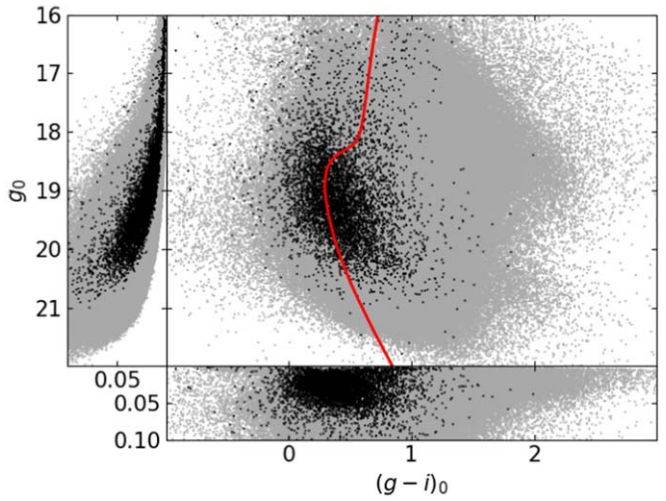

Figure 2. Color–magnitude diagram for all the measured stars in the field of NGC 6355, with their respective photometric errors. Black and gray dots represent stars located inside and outside a circle of radius equals to three times the cluster's half-mass radius (0.022 deg), respectively. The red line is an isochrone for the cluster astrophysical properties (Souza et al. 2023).

3. Data Analysis

With the aim of disentangling whether NGC 6355 presents tidal tails, we need to construct a stellar density map from stars sharing cluster features. Since selecting stars placed along the cluster main sequence can incur in a misleading analysis, because of the large amount of field stars superimposed on it, we decided to first explore the distribution of Milky Way stars across the entire color–magnitude diagram. For that purpose, we used TRILEGAL[6] (Girardi et al. 2005), a stellar population synthesis code that allows changes in the star-formation rate,

[3] http://tdc-www.harvard.edu/wcstools/
[4] Programs kindly provided by P.B. Stetson.
[5] https://irsa.ipac.caltech.edu/
[6] http://stev.oapd.inaf.it/cgi-bin/trilegal

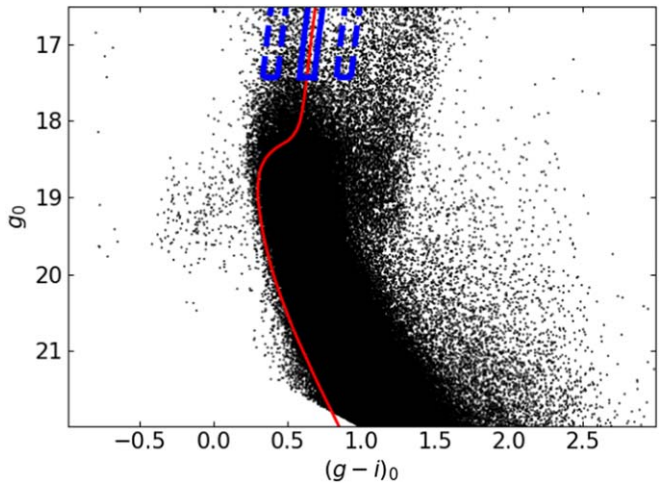

Figure 3. Synthetic Milky Way color–magnitude diagram generated using the TRILEGAL code for a circular region centered on NGC 6355 and with a radius equals to the cluster radius. The red line is an isochrone for the cluster astrophysical properties (Souza et al. 2023), while the solid and dashed blue lines enclose the selected region and two control regions, respectively.

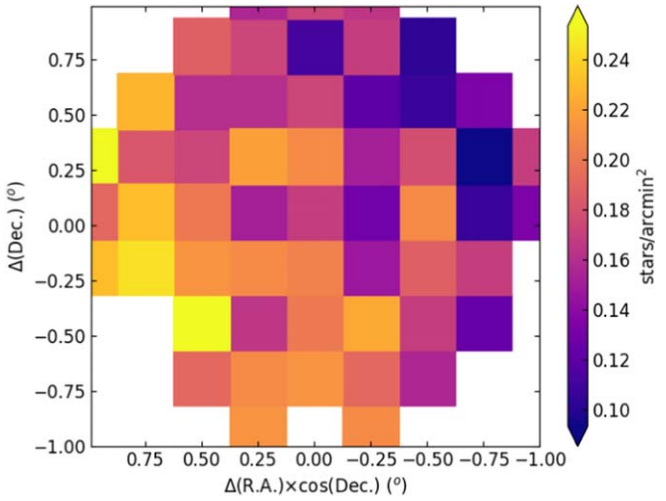

Figure 4. Milky Way synthetic stellar density map built from star counts of stars distributed within the red-giant-branch segment, generated using TRILEGAL (see text for details).

age–metallicity relation, initial mass function, geometry of Milky Way components, among others, and generated a synthetic color–magnitude diagram for a region centered on NGC 6355 with a radius equals to the cluster radius (0.1 deg; Piatti et al. 2019). The setup of the TRILEGAL code was as follows: (1) DECam photometric system, with a limiting magnitude of g, $i = 23$ mag, and a distance modulus resolution of the Milky Way components of 0.1 mag. (2) Initial mass function according to Kroupa (2002); a binary fraction of 0.3 with a mass ratio larger than 0.7. (3) Interstellar extinction modeled by an exponential disk with a scale height $h_z = 0.1$ kpc, a scale length $h_R = 3.2$ kpc, and a visual absorption variation $\partial A_V/\partial R = 0.15$ mag/kpc (Li et al. 2018), with the Sun position at $R_\odot = 8.3$ kpc and $z_\odot = 15$ pc (Monteiro et al. 2021). (4) Milky Way halo halo represented by an oblate $r^{1/4}$ spheroid with an effective radius $r_h = 2.7$ kpc, an oblateness $q_h = 0.6$, and $\Omega = 0.0001\ M_\odot/\mathrm{pc}^3$. The halo star-formation rate and age–metallicity relationship are those given by Ryan & Norris (1991). (5) Thin disk described by an exponential disk along z and R with a scale height increasing with age: $h_z = 94.7\times(1 + \mathrm{age}/5.5\times10^9)^{1.67}$, the scale length $h_R = 2.9$ kpc, and there is an outer cutoff at 15 kpc. We used a two-step star-formation rate, the age–metallicity relationship with α enrichment given by Fuhrmann (1998), and $\Sigma = 55.4\ M_\odot/\mathrm{pc}^2$. (6) Thick disk also represented by an exponential disk in both z and R directions, with scale height $h_z = 0.8$ kpc, scale length $h_R = 2.4$ kpc, and an outer cutoff at 15 kpc; $\Omega = 0.001\ M_\odot/\mathrm{pc}^3$. We adopted a constant star-formation rate and $Z = 0.008$ with $\sigma[\mathrm{M/H}] = 0.1$ dex. (7) Bulge modeled as a triaxial component with a scale length of 2.5 kpc and a truncation scale length of 95 pc, in addition to y/x and z/x axial ratios of 0.68 and 0.31, respectively. The angle between the direction along the bar and that from the Sun to the Milky Way center was set in 15 deg, and $\Omega = 406\ M_\odot/\mathrm{pc}^3$. Its star-formation rate and age–metallicity relationship were taken from Zoccali et al. (2003). The above values adopted for the different parameters are those obtained from the fits of their observed behavior so that we assumed that they reliably reproduce the different composite stellar population characteristics (Vanhollebeke et al. 2009; Girardi et al. 2012).

Figure 3 depicts the resulting Milky Way synthetic color–magnitude diagram, where we superimposed for comparison purposes a theoretical isochrone corresponding to the cluster age and metallicity. As can be seen, the red-giant branch seems to be the least cluster color–magnitude diagram contaminated region, so that we devised a segment to select stars extending from $g_0 = 16.0$ mag down to 17.5 mag and with a color width of $\Delta(g-i)_0 = 0.1$ mag. The color width resulted in a compromise between maximizing the number of cluster stars and minimizing that from field stars. We also devised two control regions placed at both sides of the red-giant-branch segment. For a more precise membership assessment within the cluster radius, we need additional information, such as proper motions, radial velocities, and metallicities. Nevertheless, field stars placed within the blue boundaries in Figure 3 are expected to be distributed smoothly varying their densities throughout the entire field (see Figure 4), so that cluster stars will arise clearly as particular shaped stellar overdensities forming an extended envelope, extra-tidal debris, or tidal tails (Piatti & Carballo-Bello 2020).

We also generated synthetic color–magnitude diagrams from the TRILEGAL code for 81 adjacent squared regions of 0.0625 deg^2 each, which cover the entire observed DECam field uniformly. From them, we counted the number of stars located within the red-giant-branch segment drawn in Figure 3, and built the corresponding stellar density map (see Figure 4). Additionally, we used the TRILEGAL squared regions and the present DECam data to build the observed stellar density map of Figure 5. These density maps are useful tools to identify extra-tidal features distributed not uniformly around the cluster's main body, as it is the case of the presence scattered debris, tidal tails, etc. This can be accomplished by subtracting from the stellar densities of Figure 5 those of Figure 4. The resulting normalized background subtracted residual stellar densities are shown in Figure 6.

Besides of using the 81 TRILEGAL squared regions, we also took advantage of the whole DECam data set to build a stellar density map of stars located within the red-giant-branch segment, employing the `scikit-learn` software machine learning library (Pedregosa et al. 2011) and its `Gaussian` kernel density estimator (KDE). We explored the bandwidth

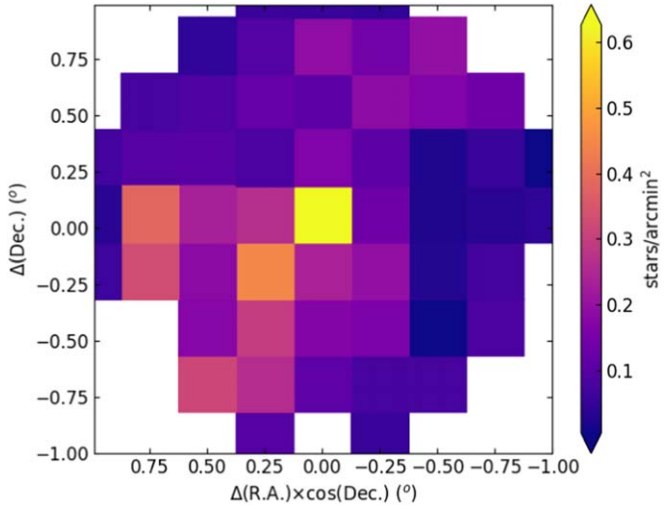

Figure 5. Same as Figure 4 using the present DECam observations.

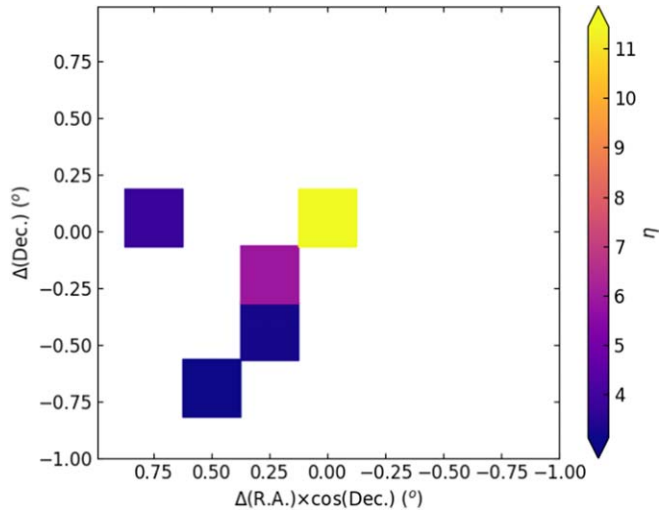

Figure 6. Map of normalized background subtracted stellar densities. Only regions with $\eta \geqslant 3$ are plotted (see text for details).

space with values from 0.01° up to 0.1° in steps of 0.01° and applied KDE for each of them using a grid of 200 × 200 boxes onto the DECam field. We finally adopted a bandwidth of 0.05° as the optimal value, as guided by `scikit-learn`. Figure 7 shows the resulting density map, once the mean background stellar density was subtracted and those values normalized to the standard deviation of the background stellar density (see Section 4 for details).

4. Analysis and Discussion

NGC 6355 is projected on to a heavily reddened region, with $E(B-V)$ values that vary from 0.65 mag up to 1.6 mag across the DECam field, as is shown in Figure 1. Figure 4 shows that the composite field stellar population also seems not to be distributed uniformly, as judged by the observed slight spatial trend in the stellar density of Milky Way red-giant-branch stars located within the devised segment of Figure 3. The observed overall increase in the stellar density and in the interstellar absorption from the northwestern to the southeastern regions of the DECam field agrees well with the direction toward the Galactic center. Curiously, the regions more severely affected by interstellar absorption are those with more red-giant-branch

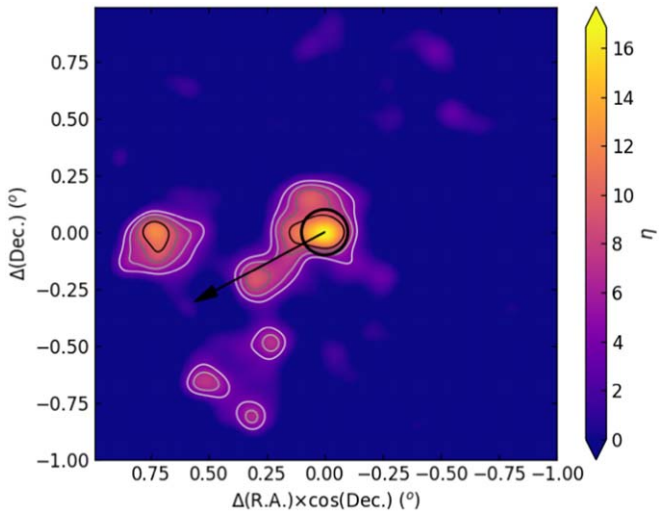

Figure 7. Map of normalized background subtracted stellar densities of stars distributed within the red-giant-branch segment (see Figure 3). Contours for $\eta = 4$, 6, 8, and 10 are drawn with with to black lines, respectively. The arrows indicates the direction to the Milky Way center. The black circle represents the cluster radius (0.1 deg; Piatti et al. 2019), which is equivalent to 14.9 pc.

segment stars. Both, variable interstellar absorption and stellar density prevent us of using the outermost region of the DECam field as the reference one to clean the field contamination in the cluster color–magnitude diagram.

We adopted a straightforward approach to clean the star counts in the cluster red-giant-branch segment from field stars across the observed DECam field (Figure 5), which consists in subtracting to the observed stellar density that measured in the Milky Way synthetic DECam field (Figure 4), for each individual squared region. In order to highlight possible cluster star overdensities throughout the DECam field, we defined a significance level as the deviation from the background level in units of its standard deviation, that is, $\eta = (\text{signal} - \text{background})/\text{standard deviation}$. We computed the mean field stellar density and its standard deviation from Figure 4, which resulted to be 0.18 ± 0.04 stars/arcmin^{-2}. We then divided the above resulting subtraction (observed—synthetic stellar densities) by 0.04, and kept significance level $\eta > 3$. Figure 6 shows that, in addition to the cluster area at the center of the DECcam field, there are also some regions toward the southeast from the cluster center that contain cluster extra-tidal stars. We applied the same procedure for the two control fields and found that none of the 81 TRILEGAL fields account for $\eta > 3$; the mean η value resulted to be -0.1 ± 0.5, which means that the adopted mean stellar background level from Figure 4 is slightly larger than that observed.

Such extra-tidal structures are clearly seen in Figure 7, where we superimposed contour levels corresponding to $\eta = 4$, 6, 8, and 10 using gray-colored lines, so that the darken the line the higher the stellar density. The cluster radius and the direction toward the Galactic center are also indicated with a black circle and an arrow, respectively. Inside the cluster radius, we found overdensities above the mean stellar field density larger than 16 times its standard deviation. As can be seen, NGC 6355 presents an extra-tidal extended envelope azimuthally not symmetric, a tidal tail, and scattered stellar debris alongside the tidal tail. As far as we are aware, this is the first Milky Way budge globular cluster with detected extra-tidal structures.

The outcome is somehow surprising according to the theoretically expected scenario. Mestre et al. (2020) compared the behavior of simulated streams embedded in chaotic and regular regions of the phase space and found that typical gravitational potentials of host galaxies can sustain chaotic orbits, which in turn do reduce the time interval during which streams can be detected. This explains why tidal tails in some globular clusters are washed out after they are generated to the point at which it is impossible to detect them. NGC 5139, with a Galactocentric distance of 6.5 kpc, has been until now the innermost globular cluster with observed tidal tails (Piatti & Carballo-Bello 2020); NGC 63655 is at 0.93 kpc from the Galactic center (Baumgardt & Vasiliev 2021). According to the cluster's angular momentum along the direction perpendicular to the Galactic plane (Souza et al. 2023), the mass of the Milky Way bulge (Valenti et al. 2016), and the regime of chaotic orbits given by Caranicolas & Papadopoulos (2003), NGC 6355 can be added to the group of objects with chaotic orbits.

At the present time, it is still a topic of debate the presence of tidal tails in some globular clusters and the absence of them in others. Piatti & Carballo-Bello (2020) explored different structural and kinematical parameter spaces, and found that globular clusters behave similarly, irrespective of the presence of tidal tails or extended envelopes, or the absence thereof. Zhang et al. (2022) showed that globular clusters with extended envelopes or tidal tails have apogalactocentric distances $\gtrsim$ 5 kpc, a behavior previously noticed by Piatti (2021), who suggested that the lack of detection of tidal tails in bulge globular clusters could be due to the reduced diffusion time of tidal tails by the kinematically chaotic nature of the orbits of these globular clusters (Kundu et al. 2019), thus shortening the time interval during which the tidal tails can be detected. Recently, Weatherford et al. (2023) reexamined the behavior of potential escapers in globular clusters dynamically evolving along chaotic orbits and found diffusion times shorter than 100 Myr. If this were the case for NGC 6355, the observed tidal tails would reveal an ongoing disruption mass process. The tidal tails in NGC 6355 points to the direction toward the Galactic center, which coincides with the theoretical predictions for the innermost parts of tidal tails (Montuori et al. 2007).

Recently, Grondin et al. (2024) generated a catalog of globular cluster extra-tidal mock stars from simulations of three-body dynamical encounters in globular cluster cores. The catalog provides celestial coordinates, proper motions, radial velocities, the actions J_R, J_z, and J_ϕ, among other stellar properties for each simulated star. These features were obtained by integrating stellar orbits in seven Milky Way scenarios where static and time-varying gravitational potentials, the structure of the disk, the shape of the dark matter halo, and the perturbations of the Large Magellanic Cloud are considered. They found that the relations between different actions are similar for cluster stars and for those stars belonging to their tidal tails. Particularly, the plane J_ϕ/J_{tot} versus $(J_z - J_R)/J_{tot}$, where $J_{tot} = J_R + |J_\phi| + J_z$, resulted to be the most suitable for identifying cluster stars distributed in their tidal tails. We computed the mean and dispersion of both ratios for mock stars generated by Grondin et al. (2024) located within a radius equals to the NGC 6255 radius, and then filtered all the mock stars located within the DECam field. Figure 8 illustrates the resulting spatial distribution of cluster and extra-tidal mock stars with action ratios within 1σ the cluster mean values. As can be seen, the presence of tidal tails is revealed, with that toward the southeast resembling the observed one (see Figure 7). Nevertheless, when comparing Figure 7 and 8 some difference remains; namely, the lack of an observed northwestern tail, and the appearance of a scattered observed extra-tidal debris located eastward of the cluster.

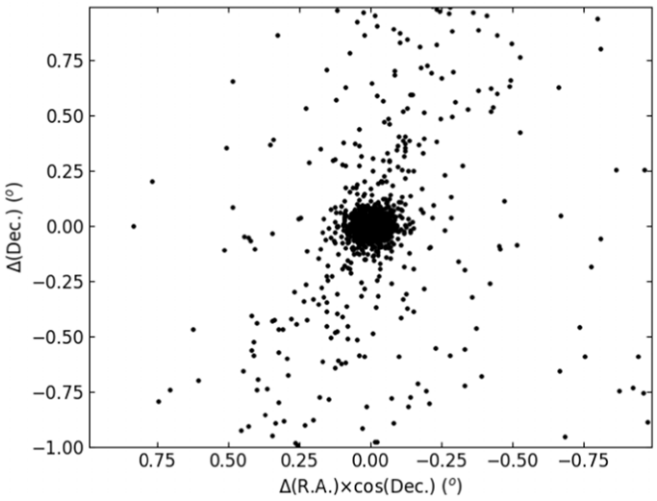

Figure 8. Spatial distribution of stars with action ratios within 1σ the cluster mean values. Data points arise from the Grondin et al. (2024)'s models.

Models of the formation and evolution of extra-tidal features around Milky Way globular clusters have also been computed by Ferrone et al. (2023). They used a set of codes called globular clusters' tidal tails to simulate streams that vary with the Milky Way potential by making use of three different profiles, either containing a central spheroid, not containing one, or containing a stellar bar. Ferrone et al. (2023) analyzed 159 globular clusters, for which 6D phase-space information, masses, and sizes are available, and classified the simulated extra-tidal structures as main tidal structures if the fraction of stripped stars from the globular cluster is larger than 10%. They analyzed 40 out of the 42 bulge globular clusters classified by Callingham et al. (2022), and 36 of them present main tidal structures, including NGC 6355. This implies that tidal tails among bulge globular clusters seem to be a more common phenomenon that previously thought. In this sense, NGC 6355 arises as the first bulge globular clusters for which its outermost regions are studied with the aim of identifying extra-tidal features. The outcomes by Ferrone et al. (2023) point to the need of observational campaigns and data analysis strategies of Milky Way globular clusters to explore their outskirts. Such data will help confirming and improving the current theoretical inputs of numerical simulations, and hence also our knowledge of the formation and evolution of the Milky Way.

5. Conclusions

We analyzed wide-field DECam g and i imaging around the Milky Way bulge globular cluster NGC 6355, with the aim of searching for extra-tidal structures. The cluster was observed as part of our CTIO 4 m Blanco telescope 2023A–627924 observing program, thus obtaining relatively deep photometry of the cluster's outskirts. Because of the heavy differential reddening and crowded star field population along the cluster line of sight, and the superposition of field stars on to the cluster color–magnitude diagram, we devised an analysis

strategy that minimizes those effects. Interstellar extinction was properly corrected using reddening values retrieved from the NASA/IPAC Infrared Science Archive, while the presence of field stars in the cluster color–magnitude diagram was constrained by selecting the least contaminated region at the upper observed part of the cluster red-giant branch. Such a red-giant-branch segment was chosen from the inspection of synthetic color–magnitude diagrams generated using the TRILEGAL code.

The stellar density map built using the synthetic star field density spatial distribution to decontaminate the observed one reveals the presence of extra-tidal overdensities above the mean stellar field density, which are between 4 and 6 times larger than the star field density dispersion. The extra-tidal stellar overdensities comprise those of an extended envelope, a tidal tail, and scattered debris; the tidal tail pointing to the direction toward the Milky Way center. We compared our results with two recent independent catalogs of simulated tidal tails around globular clusters, and confirmed the present identification of tidal tails around NGC 6355; although previous theoretical speculations discouraged the possibility to detect them because they were meant to be washed out after they were generated.

The advance produced in the generation of synthetic tidal tail features of any Milky Way globular cluster urge us to carry out observational surveys of the outskirts of globular clusters, particularly those still not studied, with the aim of providing a robust observational counterpart for the simulations, which will result in a feedback to the physics considered in the computational generation of tidal tails. In this work, we provide a first example of such an endeavor, confirming that the observed tidal tails of NGC 6355 are also predicted by numerical simulations.

Acknowledgments

We thank the referee for the thorough reading of the manuscript and timely suggestions to improve it.

This project used data obtained with the Dark Energy Camera (DECam), which was constructed by the Dark Energy Survey (DES) collaboration. Funding for the DES Projects has been provided by the US Department of Energy, the US National Science Foundation, the Ministry of Science and Education of Spain, the Science and Technology Facilities Council of the United Kingdom, the Higher Education Funding Council for England, the National Center for Supercomputing Applications at the University of Illinois at Urbana-Champaign, the Kavli Institute for Cosmological Physics at the University of Chicago, Center for Cosmology and Astro-Particle Physics at the Ohio State University, the Mitchell Institute for Fundamental Physics and Astronomy at Texas A&M University, Financiadora de Estudos e Projetos, Fundação Carlos Chagas Filho de Amparo à Pesquisa do Estado do Rio de Janeiro, Conselho Nacional de Desenvolvimento Científico e Tecnológico and the Ministério da Ciência, Tecnologia e Inovação, the Deutsche Forschungsgemeinschaft, and the Collaborating Institutions in the Dark Energy Survey.

The Collaborating Institutions are Argonne National Laboratory, the University of California at Santa Cruz, the University of Cambridge, Centro de Investigaciones Enérgeticas, Medioambientales y Tecnológicas-Madrid, the University of Chicago, University College London, the DES-Brazil Consortium, the University of Edinburgh, the Eidgenössische Technische Hochschule (ETH) Zürich, Fermi National Accelerator Laboratory, the University of Illinois at Urbana-Champaign, the Institut de Ciències de l'Espai (IEEC/CSIC), the Institut de Física d'Altes Energies, Lawrence Berkeley National Laboratory, the Ludwig-Maximilians Universität München and the associated Excellence Cluster Universe, the University of Michigan, NSF's NOIRLab, the University of Nottingham, the Ohio State University, the OzDES Membership Consortium, the University of Pennsylvania, the University of Portsmouth, SLAC National Accelerator Laboratory, Stanford University, the University of Sussex, and Texas A&M University.

Based on observations at Cerro Tololo Inter-American Observatory, NSF's NOIRLab (NOIRLab Prop. ID 2023A-627924; PI: A. Piatti), which is managed by the Association of Universities for Research in Astronomy (AURA) under a cooperative agreement with the National Science Foundation.

Data for reproducing the figures and analysis in this work will be available upon request to the author.

ORCID iDs

Andrés E. Piatti https://orcid.org/0000-0002-8679-0589

References

Baumgardt, H., & Vasiliev, E. 2021, MNRAS, 505, 5957
Callingham, T. M., Cautun, M., Deason, A. J., et al. 2022, MNRAS, 513, 4107
Caranicolas, N. D., & Papadopoulos, N. J. 2003, A&A, 399, 957
Carballo-Bello, J. A., Gieles, M., Sollima, A., et al. 2012, MNRAS, 419, 14
Carballo-Bello, J. A., Sollima, A., Martínez-Delgado, D., et al. 2014, MNRAS, 445, 2971
de Boer, T. J. L., Gieles, M., Balbinot, E., et al. 2019, MNRAS, 485, 4906
Ferrone, S., Di Matteo, P., Mastrobuono-Battisti, A., et al. 2023, A&A, 673, A44
Flaugher, B., Diehl, H. T., Honscheid, K., et al. 2015, AJ, 150, 150
Fuhrmann, K. 1998, A&A, 338, 161
Gaia Collaboration, Brown, A. G. A., Vallenari, A., et al. 2018, A&A, 616, A1
Girardi, L., Barbieri, M., Groenewegen, M. A. T., et al. 2012, Astrophysics and Space Science Proceedings, Vol. 26, Red Giants as Probes of the Structure and Evolution of the Milky Way, 165
Girardi, L., Groenewegen, M. A. T., Hatziminaoglou, E., & da Costa, L. 2005, A&A, 436, 895
Gran, F., Zoccali, M., Saviane, I., et al. 2022, MNRAS, 509, 4962
Grondin, S. M., Webb, J. J., Lane, J. M. M., Speagle, J. S., & Leigh, N. W. C. 2024, MNRAS, 528, 5189
Hozumi, S., & Burkert, A. 2015, MNRAS, 446, 3100
Kader, J. A., Pilachowski, C. A., Johnson, C. I., et al. 2023, ApJ, 950, 126
Kroupa, P. 2002, Sci, 295, 82
Kundu, R., Fernández-Trincado, J. G., Minniti, D., et al. 2019, MNRAS, 489, 4565
Li, L., Shen, S., Hou, J., et al. 2018, ApJ, 858, 75
Lindegren, L., Hernández, J., Bombrun, A., et al. 2018, A&A, 616, A2
Mackey, A. D., Ferguson, A. M. N., Huxor, A. P., et al. 2019, MNRAS, 484, 1756
Mestre, M., Llinares, C., & Carpintero, D. D. 2020, MNRAS, 492, 4398
Monteiro, H., Barros, D. A., Dias, W. S., & Lépine, J. R. D. 2021, FrASS, 8, 62
Montuori, M., Capuzzo-Dolcetta, R., Di Matteo, P., Lepinette, A., & Miocchi, P. 2007, ApJ, 659, 1212
Pedregosa, F., Varoquaux, G., Gramfort, A., et al. 2011, Journal of Machine Learning Research, 12, 2825
Piatti, A. E. 2021, MNRAS, 505, 3033
Piatti, A. E., & Carballo-Bello, J. A. 2020, A&A, 637, L2
Piatti, A. E., Carballo-Bello, J. A., Mora, M. D., et al. 2020, A&A, 643, A15
Piatti, A. E., Illesca, D. M. F., Massara, A. A., et al. 2023, MNRAS, 518, 6216
Piatti, A. E., Webb, J. J., & Carlberg, R. G. 2019, MNRAS, 489, 4367
Ryan, S. G., & Norris, J. E. 1991, AJ, 101, 1865
Schlafly, E. F., & Finkbeiner, D. P. 2011, ApJ, 737, 103
Sollima, A. 2020, MNRAS, 495, 2222
Souza, S. O., Ernandes, H., Valentini, M., et al. 2023, A&A, 671, A45
Starkman, N., Bovy, J., & Webb, J. J. 2020, MNRAS, 493, 4978

Stetson, P. B., Davis, L. E., Crabtree, D. R., et al. 1990, in ASP Conf. Ser. 8, CCDs in Astronomy, ed. G. H. Jacoby (San Francisco, CA: ASP), 289
Valenti, E., Zoccali, M., Gonzalez, O. A., et al. 2016, A&A, 587, L6
Vanhollebeke, E., Groenewegen, M. A. T., & Girardi, L. 2009, A&A, 498, 95
Wan, Z., Arnold, A. D., Oliver, W. H., et al. 2023, MNRAS, 519, 192
Wan, Z., Oliver, W. H., Baumgardt, H., et al. 2021, MNRAS, 502, 4513
Wang, S., & Chen, X. 2019, ApJ, 877, 116
Weatherford, N. C., Rasio, F. A., Chatterjee, S., et al. 2023, arXiv:2310.01485
Zhang, S., Mackey, D., & Da Costa, G. S. 2022, MNRAS, 513, 3136
Zoccali, M., Renzini, A., Ortolani, S., et al. 2003, A&A, 399, 931